Journal of Materials Chemistry A

Accepted Manuscript

This is an *Accepted Manuscript*, which has been through the Royal Society of Chemistry peer review process and has been accepted for publication.

Accepted Manuscripts are published online shortly after acceptance, before technical editing, formatting and proof reading. Using this free service, authors can make their results available to the community, in citable form, before we publish the edited article. We will replace this *Accepted Manuscript* with the edited and formatted *Advance Article* as soon as it is available.

You can find more information about *Accepted Manuscripts* in the Information for Authors.

Please note that technical editing may introduce minor changes to the text and/or graphics, which may alter content. The journal's standard Terms & Conditions and the Ethical guidelines still apply. In no event shall the Royal Society of Chemistry be held responsible for any errors or omissions in this *Accepted Manuscript* or any consequences arising from the use of any information it contains.

ROYAL SOCIETY OF CHEMISTRY

www.rsc.org/materialsA

Please do not adjust margins

Journal of Materials Chemistry A

PAPER

An adaptive supramolecular organic framework for highly efficient separation of uranium via in situ induced fit mechanism

Received 00th January 20xx,
Accepted 00th January 20xx

DOI: 10.1039/x0xx00000x

www.rsc.org/

Bo Li, Chiyao Bai, Shuang Zhang, Xiaosheng Zhao, Yang Li, Lei Wang, Kuan Ding, Xi Shu, Shoujian Li* and Lijian Ma*

On the basis of the unusual coordination structure of UO_2^{2+} combined with the adaptive nature of supramolecular organic frameworks (SOFs), here we designed and prepared a novel SOF-based solid phase extaction adsorbent (MA-TMA) using N-donor-containing melamine (MA) and O-donor-containing trimesic acid (TMA) as bifunctional building blocks mutually linked via hydrogen bonds. The as-prepared MA-TMA, with rich N-/N- and N-/O-heterocyclic structure throughout its framework, provide accessible coordination geometry and/or ligand environment for uranyl ion, which builds the crucial structural basis for the pre-organized adaptive frameworks closely related to the "induced-fit" and selective recognition of uranyl ion. The main results are as follows: 1) The highest selectivity of 92%, so far unreported, and a considerable capacity of 324 mg g^{-1} for uranium adsorption by MA-TMA are observed in weak acidic multi-cation solution (pH 2.5), accompanying with a distribution coefficient K_d value of 16000 mL g^{-1}, 100-fold or more over other 11 competitive cations; 2) MA-TMA could reach its limiting saturation capacity of 1028 mg g^{-1} at pH 4.5 in pure-U(VI) solution; 3) Noteworthily, the morphology of MA-TMA changed from the ribbon-like structure in nano-diameter before adsorption into the aggregated granules with a size of tens of microns after adsorption, which would be much more favorable for subsequent solid-liquid separation. Furthermore, possible mechanisms for the selective recognition of uranyl ions and the morphological changes of MA-TMA after adsorption are explored based on experimental characterization and chemical rationale.

1. Introduction

Uranium is both a key element for nuclear energy production and a heavy metal with higher chemical and biological toxicity, and also slightly radiological toxicity.[1-3] Thus highly efficient separation and recovery of uranium from various uranium-containing aqueous systems, especially in the whole nuclear fuel cycle from ore to wastes, is of great practical and academic significance for the purpose of sustainable development of nuclear power, human health, environment protection and resource recycling.

Since the world's first nuclear reactor has operated successfully for more than 70 years, considerable efforts have been spent in designing and synthesizing of various solid-phase extraction (SPE)/or adsorption materials for separation/extraction of uranium: from the earlier developed clay minerals (montmorillonite, bentonite and zeolite),[4-7] metal oxides (hydrated ferric oxide and magnesium oxide),[5, 8] organic ion exchange materials,[9, 10] phosphate and/or pyrophosphate (zirconium phosphate, titanium phosphate and their derivatives),[11, 12] ion imprinted polymer,[13, 14], fiber adsorbents[15-17] to recently emerged a variety of functionalized adsorbent materials which prepared by modification of solid phase matrix, such as amidoxime-functionalized mesoporous carbon, hydrothermal carbon and nanofibrous,[18-20] organosilica-phosphonate-functionalized SBA-15,[21] dihydroimidazole functionalized SBA-15,[22] salicylideneimine-functionalized hydrothermal carbon and benzimidazole-functionalized covalent organic frameworks (COF),[2, 23] and even to the latest reported layered metal sulfides,[1] metal-organic frameworks,[24-26] engineered protein,[27] iron nanoparticle,[28] polysulfide/layered double hydroxide composites,[29] and so on. However, the vast majority of the reported SPE materials for uranium, so far as we know, could not reach the desired or intended performance in high selectivity and capacity for uranium and a potential ability for practical applications, and thus leave much to be desired.

Up to now, research on the topic of uranium-selective SPE sorbents are predominantly focused on the choice of appropriate solid-phase matrixes and functional components or ligands,[18, 19, 21, 23, 26, 29] as well as related surface modification and functionalization (such as impregnating,[21] grafting,[30] embedding,[31] direct synthesis,[32] and so on). However, the "induced-fit recognition" concept established for substrate-enzyme interactions in biology is borrowed in our research work for exploring new uranium-specific SPE materials. On the basis of the unusual coordination structure of guest uranyl ion, which bears two axial oxygen atoms and 4 to 6 accessible coordination sites in the equatorial position,[33] we try a different

College of Chemistry, Sichuan University, Key Laboratory of Radiation Physics & Technology, Ministry of Education, № 29 Wangjiang Road, Chengdu, 610064, P. R. China. Fax: 86 28 85412907; Tel: 86 28 85412329; E-mail: sjli000616@scu.edu.cn (S. Li) and ma.Lj@163.com

† Electronic Supplementary Information (ESI) available: Section 1-2, Fig. S1–S8 and Table S1-S6 (Preparation of U(VI) stock solution, La(III) test solution and multi-ion solution, XPS spectra of C 1s, operating parameters for ICP-AES, different experimental conditions and adsorption capacity of U(VI), composition of the simulated nuclear industrial effluent, kinetic and thermodynamic parameters, ^{1}H NMR spectra, powder X-ray diffraction(PXRD), derivative thermal gravimetric (DTG) curve, uranium(VI) species distribution. See DOI: 10.1039/b000000x/

Journal of Materials Chemistry A Accepted Manuscript

strategy in this work. Specific host substrate, supramolecular organic frameworks (SOFs),[34, 35] that has great potential ability to match the structural characteristics of uranyl ion for complexation, was selected to prepare new and "intelligent" SPE adsorbents with high selective recognition and large adsorption capacity toward uranyl ions.

SOFs materials have been recognized as a new type of functional materials which have constructed from organic building blocks assembled via noncovalent interactions (e.g., hydrogen bonds (O–H···N and O–H···O), π···π stacking, C···H···π , and van der Waals interactions).[34] SOFs possess not only conventional properties of polymeric materials, but also distinctive structure features with accompanying new functions. Especially, the reversible, soft and flexible nature of their intermolecular interactions and the relatively easy way to find appropriate functionalized organic molecules as the building blocks makes SOFs materials have recently attracted increasing interest in the field of molecular recognition,[36-38] gas adsorption and storage,[39-41] drug delivery,[42, 43] fluorescent sensing,[44] and so on. However, to the best of our knowledge, the rational design and utility of SOFs for selective separation of uranium from aqueous solutions have, so far, remained fairly unexplored and is yet an interesting topic.

Herein, N-donor-containing melamine (MA) and O-donor-containing trimesic acid (TMA) were employed, as bifunctional building blocks and ligands, to prepare the expected SOF material (MA-TMA) via one-step hydrogen-bond-driven self-assembly. The interactions between MA and TMA afforded rich heterocyclic structures in the SOF-based SPE adsorbents with abundant and multi-sites N, O ligands for the guest uranyl. The results of batch adsorption studies indicated that the MA-TMA displayed both superior recognition performance and prominent capacity in extraction/adsorption of UO_2^{2+} from multi-ion metal solutions. Besides, a possible mechanism for induced-fit uranyl recognition of MA-TMA was explored.

2. Experimental Section

2.1 Materials

MA and TMA were purchased from Aladdin Chemistry Co., Ltd., China. All metal oxides or nitrates were purchased from Aladdin Chemistry Co., Ltd., China. Other organic reagents, including dimethylsulfoxide (DMSO), ethanol and acetone were purchased from Chengdu Forest Science & Technology Development Co., Ltd., China. All reagents were of AR grade and were used without further purification.

2.2 Characterization methods

Fourier transform infrared (FT-IR) spectra were obtained from Perkin-Elmer IR-843 spectrometer. Scanning electron microscope (SEM) were performed using a JEOL-JSM-7. Thermal gravimetric analysis (TGA) and derivative thermal gravimetric (DTG) were performed under nitrogen atmosphere using a SDT Q600 thermogravimetric analyzer with a flow rates of 20 mL min^{-1} and a heating rate of 10 °C min^{-1}. Elemental analyzer (EA) was performed on a Carlo-Erba 1106 elemental analyzer. Nuclear magnetic resonance (NMR) spectra were collected in DMSO using a Bruker 400 MHz spectrometer at a resonance frequency of 400 MHz for ^1H. X-ray photoelectron spectroscopy (XPS) measurements were conducted on a XSAM800 spectrometer with a monochromatic Al X-ray source operated at 300 W. Powder X-ray diffraction (PXRD) patterns were recorded on a DX-1000 instrument operated at 40 Kv and 25 mA, using Cu Kα radiation. Solid-state diffuse reflectance UV-vis spectra were obtained at room temperature on a Shimadzu UV-3600 double beam spectrophotometer in the wavelength range of 200-1100 nm. Inductively coupled plasma atomic emission spectroscopy (ICP-AES) (Thermo Elemental, USA) were used to analyze the initial and equilibrium concentration of U(VI) and other metal ions in the solution. Standard curve method has been used in ICP-AES measurement for the determination of the metal ion concentration in test samples. The standard curve, obtained by using diluted nitric acid solution (6%) to dilute the uranium or uranium-containing stock solution. The standard curve for uranium concentration determination is established using uranium standard solution with different concentration of 0, 20, 40, 60 ppm, respectively. The calibration plot was linear in the investigated concentration range with the correlation coefficient greater than 0.999. The operating parameters for the ICP-AES are described in Electronic Supplementary Information (ESI) Table S1†.

2.3 Preparation of MA-TMA

In order to investigate the effect of synthesis conditions on uranium adsorption by MA-TMA, several parameters (reaction time, temperature, molar ratio, and so on) were chosen, and the detail experimental conditions and adsorption results were listed in Table S2, 3†. Briefly, MA (0.63 g, 5 mmol) and TMA (0.21 g, 1 mmol) were dissolved in 50 ml of hot DMSO respectively. After complete dissolution, the hot DMSO solution of TMA was then added dropwise into the hot DMSO solution of MA. The mixture was left under stirring at 353 K for 2 h, after which a white flocculent precipitate was obtained by the gradual addition of deionized water. The as-prepared material was then washed thoroughly with deionized water, ethanol and acetone alternately. The final white solid powder (inset in Fig. 12) was dried in a vacuum oven for 12 h at 323 K and denoted as MA-TMA.

2.4 Batch adsorption experiments

10 mg of adsorbent was added into a 50 mL Erlenmeyer flasks along with 25 mL of either pure U(VI) or La(III) solution or a simulated nuclear industrial effluent sample containing 12 co-existing cations (Table S4†) with designed metal ion concentration and pH value. Simulated nuclear industrial effluent samples were prepared mainly based on the composition of a typical nuclear power reactor effluent.[13] More detailed information on preparation of U(VI), La(III) and multi-ions stock solution can be found in ESI Section S1†). All samples were shaken for a certain time (*t*, min) at specified temperatures (*T*, K). Then the solid was separated from supernatant by centrifugation, and the concentrations of metal ions in the supernatant, before and after adsorption, were determined by ICP-AES. All samples were tested at least twice during ICP-AES measurements. The U(VI)-loaded MA-TMA samples obtained under

Journal of Materials Chemistry A Accepted Manuscript

 This journal is © The Royal Society of Chemistry 20xx

Please do not adjust margins

the condition of C_o = 300 mg L^{-1}, v = 150 mL, ω = 10 mg, T = 298 K with three parallel samples were washed thoroughly with deionized water until the filtrate was nearly neutral followed by drying in a vacuum oven at 323 K for 12 h. The as-produced yellow powder (inset in Fig. 12) was denoted as MA-TMA-U. Similarly, the La-loaded MA-TMA was obtained by using a test solution containing only lanthanide (III) species for a comparison of the morphology change of the adsorbent after uranium adsorption, and denoted as MA-TMA-La. Adsorption capacity (q_e, mg g^{-1}) of either U(VI) or other metal ions and distribution coefficient K_d (mL g^{-1}) were calculated by the following equations (1) and (2):[18]

$$q_e = \frac{(c_0 - c_e)\times V}{\omega} \quad (1)$$

$$K_d = \frac{(c_0 - c_e)\times V}{c_e \times \omega} \quad (2)$$

where C_o and C_e are the initial and equilibrium concentrations of metal ion (mg L^{-1}), respectively; V is the volume of testing solution (L); and ω is the weight of adsorbent (g).

A specific term, Uranium-selectivity (S_U), was coined to describe the potency and degree of the selectivity of the adsorbents to uranium:[18, 32]

$$S_U = \frac{q_{e\text{-}U}}{q_{e\text{-}tol}} \times 100\% \quad (3)$$

where $q_{e\text{-}U}$ is the amount of uranium adsorbed (mmol g^{-1}) and $q_{e\text{-}tol}$ is amount of all cations adsorbed (mmol g^{-1}) in multi-ion solution. All glassware was soaked in 10.0 wt% HNO_3 solution for 12 h before used to remove any metal impurities which might be adsorbed on the walls of glassware. All tests were carried out at least in duplicates.

3. Results and discussions

3.1 Characterization

3.1.1 FT-IR and ^{1}H NMR

Fig. 1 shows the FT-IR spectra of MA, TMA, MA-TMA and MA-TMA-U. In the FI-IR spectrum of MA, the peaks at 3469 and 3417 cm^{-1} are typical NH_2 stretch peaks.[45] Contrastively, these peaks in spectrum of MA-TMA are broader and smoother and located at 3427 cm^{-1}. The disappearance of N-H vibration peaks suggest the formation of hydrogen bond between MA and TMA.[46] Furthermore, the triazine ring vibration of MA moves from 815 cm^{-1} to 791 cm^{-1}, and the C=O stretching peak of TMA shifts from 1719 cm^{-1} to 1695 cm^{-1}, which also demonstrate the formation of hydrogen bond between MA and TMA.[47, 48] The appearance of a broad band around 3197 cm^{-1} is due to asymmetric and symmetric O–H stretching modes and a band in the range 1600–1585 cm^{-1} is due to H–O–H bending vibration,[49] indicating the presence of water molecules (chemically and physically adsorbed water), which is further confirmed by TGA and XPS studies. Furthermore, the FT-IR spectrum of the MA-TMA-U (Fig. 1) exhibits the existence of a new peak at ~922.3 cm^{-1} assigned to the antisymmetric vibration of the $[O=U^{VI}=O]^{2+}$ group,[1] which is not present in the spectrum of MA-TMA (Fig. 1). Thus it is reasonable to infer that there are interactions between MA-TMA and uranyl ions.

The ^{1}H NMR results (Fig. S1†) indicated that the amino protons of MA-TMA shift downfield by 0.5 ppm compared with that of MA. Furthermore, the chemical shifts of the amino protons in DMSO are concentration-dependent. With the increasing amount of MA-TMA, the amino proton signals shift downfield (Fig. S2†). These results proved the formation of a hydrogen-bonded complex in the as-prepared MA-TMA,[50] which is consistent with the results of FI-IR studies. Comparing the ^{1}H NMR spectra of MA-TMA in the absence [Fig. 2 (a)] and in the presence of UO_2^{2+} [Fig. 2 (b)], it can be noticed that the integrated area of amino protons decreased obviously after the addition of UO_2^{2+}, which could be due to the coordination interaction of uranyl ion and amino group. In addition, the chemical shift of the amino protons and benzene protons shifts from 6.60 and 8.69 to 6.47 and 8.61 ppm, respectively. These results indicated that the uranyl ions interact not only with N of amino group, but also with O of carboxyl group. So the shielding effect increases with increasing electron cloud density around the nuclei and thus the resonance signals of the samples are shifted to a high field and the chemical shift decreases. This coordination interaction between uranium and ligands (N and O) was further verified by XPS and solid-state diffuse reflectance UV-vis.

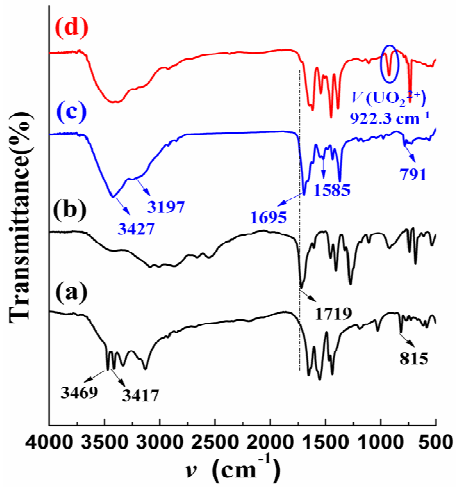

Fig. 1 FT-IR spectra of (a) MA, (b) TMA, (c) MA-TMA and (d) MA-TMA-U.

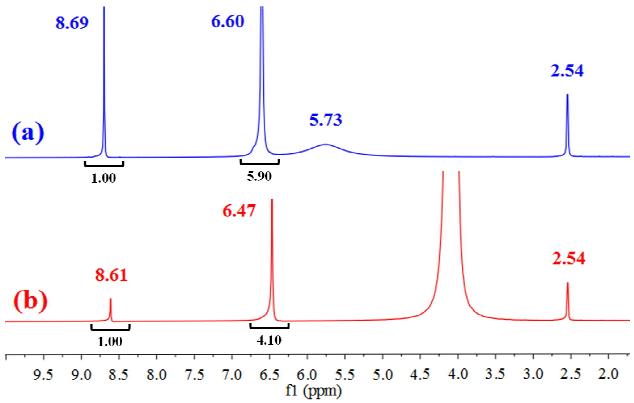

Fig. 2 ^{1}H NMR spectra of MA-TMA in the absence (a) and in the presence of (b) UO_2^{2+} (C_o = 300 mg L^{-1}, v = 80 μL) in DMSO.

Journal of Materials Chemistry A Accepted Manuscript

3.1.2 TGA and EA

The thermal properties of MA, TMA and MA-TMA are shown in Fig. 3 and Fig. S3†. The weight losses of MA and TMA occur at 264 and 310 °C, respectively. Three-stage weight losses were obviously observed in the TGA profile of MA-TMA. The first weight loss (~14.1%) appears at about 108 °C, which can be devoted to the loss of water. The remaining two weight losses occur around 245 °C and 300 °C, corresponding to the stepwise loss of MA and TMA. The weight losses of MA and TMA are 39.1 and 34.9 %, suggesting that the molar ratio of MA and TMA is 1.87 : 1. These results are basically the same as the results of elemental analysis (Table 1). Therefore, the final ratio of MA, TMA, and water in the MA-TMA may be 2:1:4, as shown in Scheme 1, which suggests that there are abundant N-/N- and N-/O-heterocyclic structures linked mutually by hydrogen bonding in the as-prepared MA-TMA.

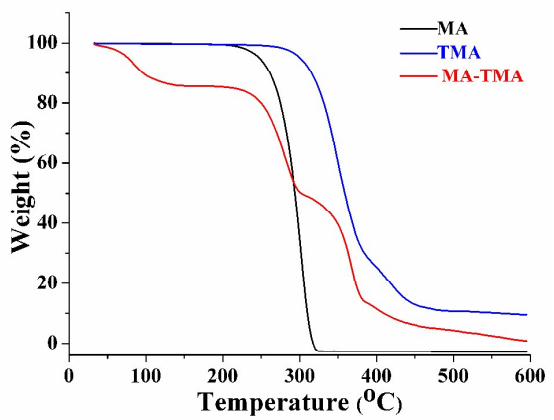

Fig. 3 TG analysis of MA, TMA, and MA-TMA.

Table 1. Ratio of elements of MA, TMA, MA-TMA by an elemental analyzer (EA)[a]

Sample	C (at %)	N (at%)	O (at %)	H (at %)
MA	28.6	66.7		4.7
TMA	51.4		45.7	2.9
MA-TMA	31.8	35.8	27.3	5.1
Calculated	33.7	31.5	29.9	4.9

[a]: Calculated from the ratio of 2:1:4 to MA, TMA and H_2O

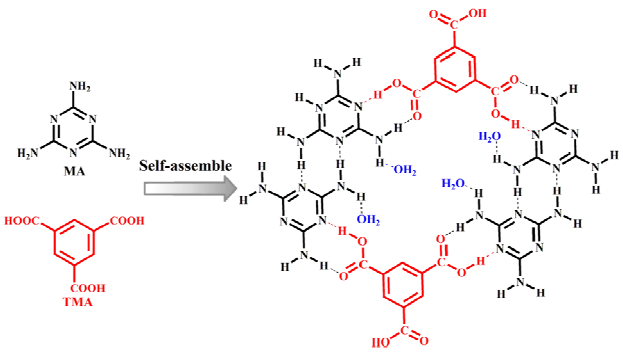

Scheme 1 Schematic illustration of a possible structure of MA-TMA.

3.1.3 SEM and PXRD

SEM investigation at lower magnification [Fig. 4(a)] shows that MA-TMA displays a ribbon-like structure that is several hundred nanometers in width, and dozens or even hundreds of micrometers in length. It is particularly gratifying that the morphology of MA-TMA changed from the ribbon-like shape before adsorption into the aggregated granules with a size of tens of microns after adsorption [Fig. 4(b)]. The aggregated granules would be much more favorable for subsequent solid-liquid separation. Two reasons may lead to such interesting changes. Firstly, during adsorption, all or part of connections between MA and TMA originally on the basis of the hydrogen bonding interaction could be replaced by the stronger covalent interaction between the uranyl ions and the N-, O-containing ligands in the heterocyclic framework in MA-TMA. Secondly, the formation of hydrogen bonds between the two axial oxygen atoms of uranyl ion and the amino and/or hydroxy groups on adjacent layers of the interwoven MA-TMA ribbon may also lead to such results. The SEM image of La(III)-loading MA-TMA with microrod-like morphology [Fig. 4(c)] and PXRD pattern of MA-TMA-La [Fig. S4†] obtained in similar batch adsorption condition provided ancillary evidence to support the above possible mechanism for the observation of aggregated MA-TMA-U granules after adsorption.

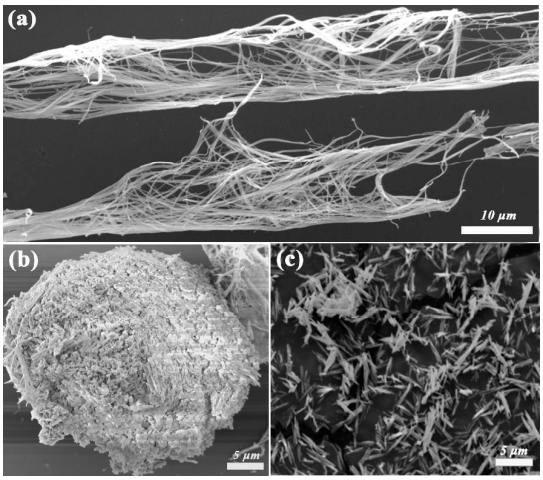

Fig. 4 SEM images of MA-TMA (a), MA-TMA-U (b) and MA-TMA-La (c).

The PXRD patterns of the solid samples in Fig. 5 show well-defined crystalline structure of MA-TMA and MA-TMA-U. Comparing the PXRD patterns of the samples before and after adsorption, it was found that two new peaks appeared around 2θ =13° and 25° in pattern of MA-TMA-U should be the characteristic peaks of the uranyl complex.[51] Meanwhile, in the pattern of MA-TMA, some peaks around 2θ =10° and 38° were shifted slightly to the left, and some peaks around 2θ =18° and 27° were shifted right slightly, suggesting the incorporation of uranyl ion into the lattice sites of the MA-TMA. The results prove that uranyl ion was extracted onto MA-TMA by chemical bonding, and relevant structural changes might occur in the MA-TMA framework.

Journal of Materials Chemistry A Accepted Manuscript

This journal is © The Royal Society of Chemistry 20xx

Please do not adjust margins

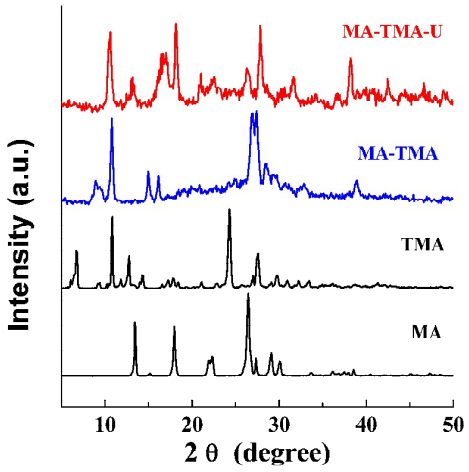

Fig. 5 Powder X-ray diffraction spectra of MA, TMA, MA-TMA and MA-TMA-U.

3.1.4 XPS and Solid-state diffuse reflectance UV-vis

XPS analyses were performed on MA-TMA and MA-TMA-U samples to provide more detailed information about the chemical changes occurring in the samples before and after uranium adsorption. Survey spectra in Fig. 6(a) indicated clearly a new strong double U4f peak in MA-TMA-U, and the corresponding high-resolution U4f$_{7/2}$ and U4f$_{5/2}$ core-level spectra [Fig. 6(c) and (d)], respectively revealed the existence of uranium(VI) in the MA-TMA-U sample.[52] The N 1s core-level peak in Fig. 6(b) shows about 1.2 eV shift to higher binding energy after the uranium loading, which testifies the chemical bonding between uranyl ions and the nitrogen atoms on MA-TMA including amino nitrogen and/or heterocyclic nitrogen atoms. In the O 1s XPS spectra of MA-TMA [Fig. 6(e)] and MA-TMA-U [Fig. 6(f)], three peaks around 531, 532 and 533 eV are attributed to C=O, C-O and adsorbed water respectively.[18] Comparing with the three O 1s core levels in each sample, it is found that the peak1 for the C=O located at 531.5 eV in Fig. 6(e) experiences a negative shift of 0.2 eV after adsorption, also the peak 2 for the C-O located at 532.8 eV in Fig. 6(e) shifts to lower binding energy by as much as 0.6 eV accompanying with remarkable decrease of the intensity of the peak after adsorption, and on the contrary, the position of the peak 3 for adsorbed water does not change as expected for the adsorption situations discussed here, which imply that there are chemical interactions between uranyl ion and the carboxylic acid (carbonyl and hydroxyl) on the as-synthesized MA-TMA.[53] More detailed information of C 1s peaks of MA-TMA and MA-TMA-U are shown in ESI, Section 2 and Fig. S5†.

The above results are further verified by solid-state diffuse reflectance UV-vis spectroscopy (Fig. 7). Firstly, the strong peak of MA-TMA shifts from 238 to 246 nm for MA-TMA-U originating from charge-transfer electronic transition within the U=O double bonds after adsorption.[54] The new shoulder peaks appear at 432, 447 and 461 nm are characteristic of uranyl absorptions,[55] which is attributed to ligand to metal charge transfer between the oxygen and nitrogen (p orbital) atoms of the coordinating ligands and an empty orbital of the uranium (6d/5f).[55] These results strongly suggested that the coordination site in MA-TMA to uranyl is most likely the nitrogen and oxygen donor atom in the N-/N- and N-/O-heterocyclic structure. A more detailed discussions about the adsorption mechanism or coordination interaction between MA-TMA and uranium have been described in section 3.2.6.

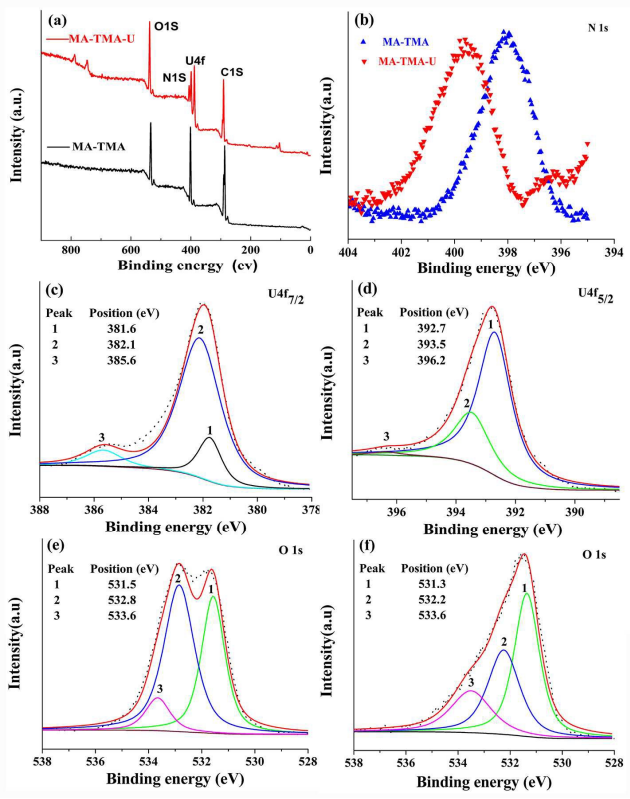

Fig. 6 (a) The typical XPS survey spectra of MA-TMA and MA-TMA-U. High resolution XPS spectra of N 1s for (b) MA-TMA and MA-TMA-U; U4f$_{7/2}$ (c) and U4f$_{5/2}$ (d) for MA-TMA-U; and O 1s for (e) MA-TMA and (f) MA-TMA-U.

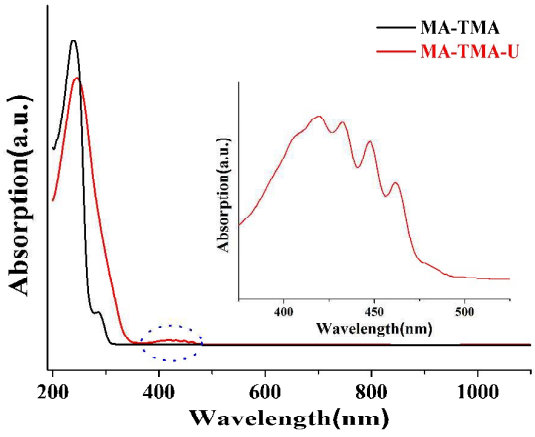

Fig. 7 Solid-state diffuse reflectance UV−vis spectra for MA-TMA and MA-TMA-U at room temperature.

Journal of Materials Chemistry A Accepted Manuscript

3.2 Extraction of uranium by MA-TMA

3.2.1 Effect of pH

According to solubility calculation and modeling of species distribution using a CHEMSPEC (C++) program,[18] uranyl ions would be converted into an insoluble specie ($UO_2(OH)_2$) at pH value higher than 4.5 in the concentration range used in this study (≤ 300 mg L^{-1}), (Fig. S6†). Therefore, the effect of pH on adsorption behavior of MA-TMA toward U(VI) was investigated in different pH values ranging from 1.0 to 4.5. The results are shown in Fig. 8. It is clear that the adsorption capacity of the MA-TMA towards uranium strongly depends on the solution pH. The adsorption capacity increases sharply with increasing pH from 1.5 to 2.5, and then slowly increases with the further increase of pH, and reaches 358 mg g^{-1} at pH 4.5. Therefore, an optimum pH value for effective separation was chosen to be around 4.5 in further studies.

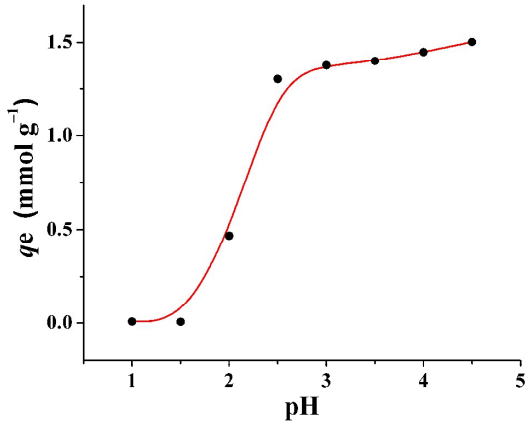

Fig. 8 Effect of pH on the adsorption of U(VI) (C_o ≈ 165 mg L^{-1}, t = 120 min, v = 25 mL, T = 298 K, and ω = 10 mg).

3.2.2 Kinetic studies

The effect of contact time on U(VI) adsorption to MA-TMA is shown in Fig. 9. The adsorption capacity of U(VI) increased linearly during the first 5 min and 10 min was found to be sufficient for reaching adsorption equilibrium. Particularly, over 64% of total adsorption capacity occurred during the first minute. These results indicate that the adsorption is a very rapid process.

Three different kinetic models, namely pseudo-first-order, pseudo-second-order model and intraparticle diffusion model were employed to evaluate the controlling mechanism of the adsorption process. The linear forms of the three models can be expressed by the following equations. (4)-(6) respectively,[32]

$$\ln(q_e - q_t) = \ln q_e - k_1 t \quad (4)$$

$$\frac{t}{q_t} = \frac{1}{k_2 q_e^2} + \frac{1}{q_e} t \quad (5)$$

$$q_t = k_{int} t^{0.5} + C \quad (6)$$

where q_t refers to the amount of U(VI) adsorbed (mg g^{-1}) at any time t, k_1 (min^{-1}) and k_2 (g mg^{-1} min^{-1}) are the pseudo-first-order and the pseudo-second-order rate constants, respectively. k_{int} (mg g^{-1} $min^{-1/2}$) is the intraparticle diffusion rate constant, and C (mg g^{-1}) is the constant proportional to the extent of boundary layer thickness.

For Eqs. (4)–(6), linear plots of ln ($q_e - q_t$) vs. t, t/q_t vs. t and q_t vs. $t^{1/2}$ are given respectively in Fig. S7† (a)–(c). The values of constants in Eqs, (4)–(6) are shown in Table S5†.

The higher correlation coefficient value (R^2 = 0.9999) with the $q_{e,cal}$ (270 mg g^{-1}) closer to the $q_{e,exp}$ (260 mg g^{-1}) suggests that the pseudo-second-order model could be used for a better description of the adsorption process. Meanwhile, the results imply that the current adsorption process might be regarded as chemiadsorption.[2]

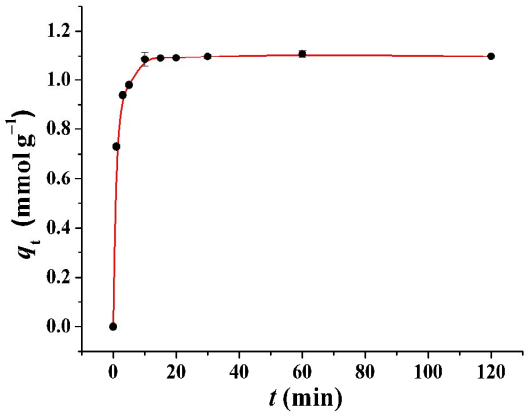

Fig. 9 Effect of contact time on the adsorption of U(VI) (C_o ≈ 100 mg L^{-1}, pH = 4.5, v = 25 mL, T = 298 K, and ω = 10 mg).

3.2.3 Thermodynamic studies

The effect of temperature on the adsorption of U(VI) onto MA-TMA is shown in Fig. 10. The adsorption capacity of U(VI) slightly decreases (about 2 mg g^{-1}) with increasing environmental temperature from 298 to 338 K, which indicate that low temperature may be favored for the adsorption of uranium onto MA-TMA. Three basic thermodynamic parameters, free energy change (ΔG), enthalpy change (ΔH) and entropy change (ΔS), were calculated using the following Eqs. (7)-(8),[2, 23] and the previously obtained experimental data, and listed in Table S6†.

According to Eq. (7), the plot of lnK_d vs. $1/T$ (Fig. S8†) showed that the K_d value decreases with increasing temperature in the range of 298 to 338 K.

$$\ln K_d = \frac{\Delta S}{R} - \frac{\Delta H}{RT} \quad (7)$$

$$\Delta G = \Delta H - T\Delta S \quad (8)$$

From the thermodynamic parameters in Table S7†, the negative values of ΔG and ΔH indicate that the adsorption of U(VI) is spontaneous and exothermic in nature. Moreover, the positive value of ΔS shows the increased randomness at the solid-solution interface during the adsorption process, which reflects the strong affinity of the adsorbent material for uranyl ions.[32]

Journal of Materials Chemistry A Accepted Manuscript

This journal is © The Royal Society of Chemistry 20xx

Please do not adjust margins

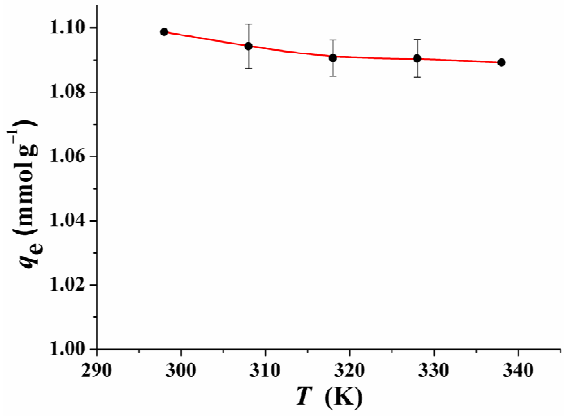

Fig. 10 Effect of temperature on the adsorption of U(VI) ($C_o \approx 100$ mg L^{-1}, pH = 4.5, v = 25 mL, t = 120 min, and ω = 10 mg).

3.2.4 Isotherm studies and limiting adsorption capacity of uranium

The amount of uranium adsorbed onto MA-TMA increases with an increase in initial uranium concentration as can be seen in Fig. 11. The saturation adsorption has not yet been reached even when uranium concentration rises up to 300 mg L^{-1} and, if the concentration in testing solution continues to increase over this point at pH 4.5, the UO_2^{2+} would be converted into hydrolysis species like UO_2OH^+ and even insoluble ($UO_2(OH)_2$) (Fig. S6†).

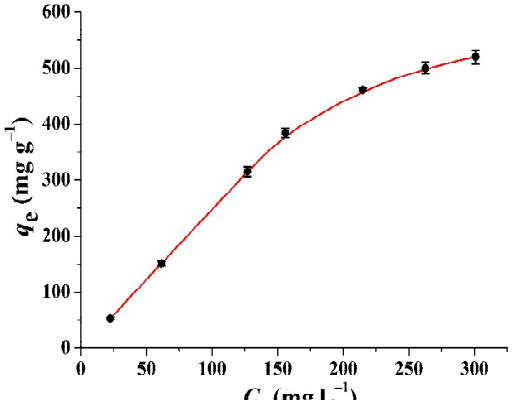

Fig. 11 Effect of initial uranium concentration on the adsorption of uranium onto MA-TMA (pH = 4.5, t = 120 min, v = 25 mL, T = 298 K, and ω = 10 mg).

Therefore, in order to investigate the limiting saturation capacity of MA-TMA towards uranium, batch adsorption experiments with an increase in uranium content in the test solution is carried out by gradually increasing the volume of the uranium solution from 25 mL to 200 mL (C_o = 300 mg L^{-1}), and keeping other adsorption conditions unchanged (pH = 4.5, ω = 10 mg, t = 2 h, and T = 298 K). The relationship between the adsorption capacity of uranium and volume of the feed solution is shown in Fig. 12. The uranium adsorption amount reaches to 2.18 mmol g^{-1} (520 mg g^{-1}) when a volume of 25 mL is used. With the increase of the volume of uranium solution, the adsorption capacity of uranium raises steadily and achieves equilibrium adsorption capacity when the solution volume increases to 150 mL. The limiting saturation adsorption capacity of MA-TMA towards uranium is found to be 1028 mg g^{-1}. This value is more than the experimentally obtained capacity of all other reported uranium sorbents so far (Table 2).

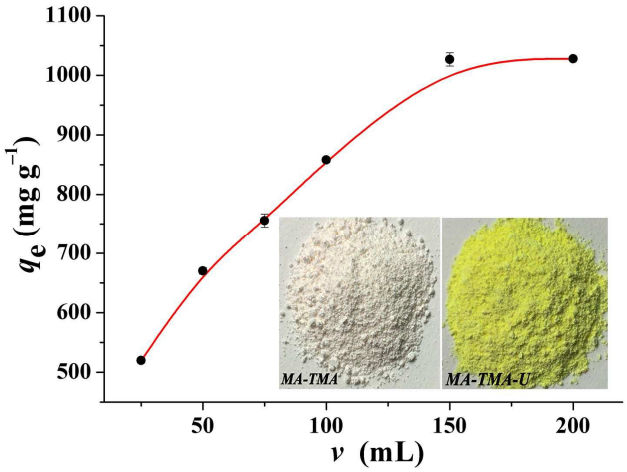

Fig. 12 Limiting adsorption capacity of U(VI) onto MA-TMA ($C_o \approx$ 300 mg L^{-1}, pH = 4.5, t = 120 min, T = 298 K, and ω = 10 mg).

Table 2 Comparison of adsorption capacity of U(VI) on various uranium adsorbents

Adsorbents	Adsorption Conditions		Adsorption Capacity (mg g^{-1})	Reference
	C_o (mg L^{-1})	pH		
Mesostructured organosilica-phosphonate hybrids	400	4.0	55.0	21
A solid supported ionic liquid (SSIL)	1000	3.0	110	30
Highly porous and stable MOF	100	2.5	217.0	26
Benzimidazole-functionlized 2-D COF	300	4.5	250.0	23
Dihydroimidazole functionalized SBA-15	290	5.0	268.0	22
MOF-76	200	3.0	298.0	56
Amino functional MOFs	200	5.5	350.0	24
Layered metal sulfides	400	3.5	380.0	1
5-azacytosine-functionalized	240	4.5	408.4	57

Journal of Materials Chemistry A Accepted Manuscript

hydrothermal carbon				
Metal silicate nanotubes	>200	~	929.0	58
Amidoxime-functionalized hydrothermal carbon	300	4.5	1021.6	18
MA-TMA	300	4.5	1028	This work

3.2.5 Selective extraction of uranium by MA-TMA

High efficient extraction and separation of uranium has always been one of the hotspots and difficulties in the field of separation science. The above results highlight the high saturated adsorption capacity of MA-TMA towards uranium, so the selective recognition and separation of U(VI) onto MA-TMA was discussed in detail via batch adsorption experiment in simulated nuclear industry effluent containing 11 competing metal cations except UO_2^{2+} ion. Some representative transition metal and alkaline earth metal ions were selected as competitive ions, including especially five typical lanthanide nuclides (La^{3+}, Sm^{3+}, Nd^{3+}, Gd^{3+}, Ce^{3+}) which usually have strong coordination capacities to functional ligands. In addition, uranium adsorption in MA-TMA is greatly dependent on solution pH as mentioned above (Fig. 8). So the selective recognition behavior of uranium at different pH values (2.0–4.5) in multi-cation solutions was studied in an attempt to better explore the relationship between pH and uranium adsorption selectivity as well as adsorption capacity.

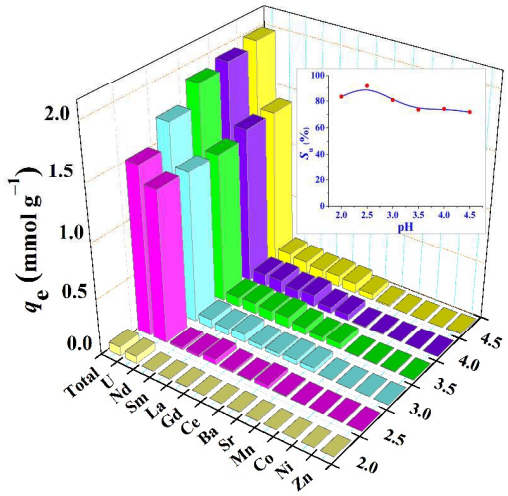

Fig. 13 Effect of pH on the adsorption of U(VI) in a multi-ion system ($C_o \approx 1.0$ mmol L^{-1} for all cations, t = 120 min, v = 25 mL, T = 298 K, and ω = 10 mg).

The results are shown in Fig. 13. This adsorption trend is consistent with the results obtained in different pH of pure uranium solution (Fig. 8). The adsorption capacity of MA-TMA towards metal ions increased sharply from pH 2.0 to 2.5 and the uranium adsorption amount occurs from 16 mg g^{-1} at pH = 2.0 to 324 mg g^{-1} at pH = 2.5. With the following increase of pH, the adsorption capacity increases slowly and the adsorption amount towards U(VI) reaches to 335 mg g^{-1} (1.4 mmol g^{-1}) when pH is 4.5, about 70 percent of the total adsorption capacity (2.00 mmol g^{-1}) for all nuclide ions in the multi-cation solution, and the K_d value for uranium reaches up to 20000 mL g^{-1} (Fig. 14). Comparing with the uranium adsorption capacity (2.18 mmol g^{-1}) in pure uranium system in the same conditions (pH = 4.5, ω = 10 mg, v = 25 mL, t = 2 h, and T = 298 K) except somewhat different initial U(VI) concentrations, 1.26 and 1.0 mmol L^{-1} for both pure uranium system and multi-ion system separately, the other competitive cations in multi-ion system have a significant effect on uranium adsorption capacity of MA-TMA.

However, it is worth noting that MA-TMA shows an unprecedented selectivity towards uranium in multi-metal bearing solutions. Throughout the pH range (2.0–4.5) studied, the uranium selectivity, S_U, is always higher than 70% (insert in Fig. 13). Distinctively, a so far unreported highest-selectivity of 92% (insert in Fig. 13) with a considerable adsorption capacity of 324 mg g^{-1} at pH 2.5, and MA-TMA offers very high affinity and selectivity for uranium with a K_d value of 16000 mL g^{-1}, 100-fold or more over other 11 competitive cations (Fig. 14). The results demonstrate that MA-TMA possesses an outstanding recognition ability for selective separation of uranium from the existing competitive ions, especially in weak acidic solutions. The excellent uranium binding affinity and selectivity make it has bright potential application prospect in separation of uranium from various uranium-containing nuclear industrial effluents.

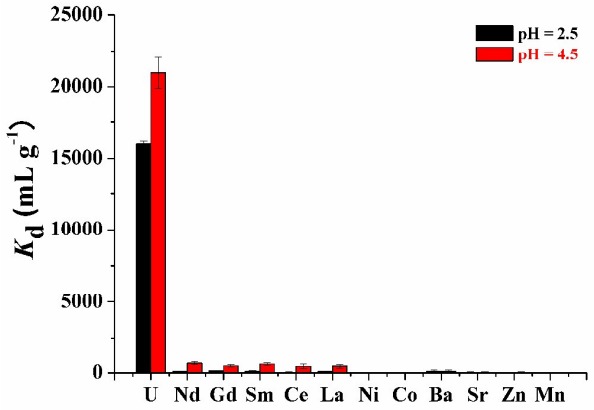

Fig. 14 The K_d values of coexistent ions on MA-TMA at different pH ($C_o \approx 1.0$ mmol L^{-1} for all cations, t = 120 min, v = 25 mL, T = 298 K, and ω = 10 mg).

3.2.6 Possible adsorption mechanism

XPS, FT-IR, PXRD, ^{1}H NMR and Solid-state UV-Vis diffuse reflectance spectra of MA-TMA and MA-TMA-U were recorded to understand the mechanism for selective recognition and extraction of uranium by MA-TMA. Firstly, for the as-synthesized MA-TMA, the significant changes in morphology (from the ribbon-like shape [Fig. 4(a)] into the aggregated granules [Fig. 4(b)]) and color (from white to the bright yellow (inset in Fig. 12) were observed after loading of uranium. It is reasonable to infer that there are interactions between

Journal of Materials Chemistry A Accepted Manuscript

This journal is © The Royal Society of Chemistry 20xx

Please do not adjust margins

MA-TMA and uranyl ions. Moreover, comparing the FT-IR spectra (Fig. 1) and PXRD patterns (Fig. 5) of the samples before and after adsorption of uranium, it further proves that the uranyl ion was extracted onto MA-TMA by chemical bonding. Finally, the ^{1}H NMR results (Fig. 2), XPS (Fig. 6) and solid-state diffuse reflectance UV-vis (Fig. 7) strongly confirm that there exist the interaction, most likely chelation, between uranyl ions and nitrogen (amino nitrogen and triazine nitrogen) and oxygen (hydroxyl oxygen and ketonic oxygen) ligands on the N-/N- and N-/O-heterocyclic structure of MA-TMA.

MA-TMA is mainly composed of a large number of mutually hydrogen-bond-linked N-/N- and N-/O-heterocyclic units. The flexible building mode provides the pre-organized coordination geometry and/or ligand environment with reversible, adaptive features for the charge-concentrated equatorial position of uranyl ion. Meanwhile, the large amount of N, O donor atoms in the heterocyclic moieties, which could act as reliable coordination sites, offer an effective guarantee to MA-TMA for the separation of uranyl in situ in the induced fit mode with highly selectivity and large capacity. Therefore, we could assume the following mechanism for the extraction of uranium by MA-TMA. When MA-TMA encounters uranyl ions in aqueous solution, the chemical structures of N-/N- and N-/O- heterocycles in MA-TMA framework would change correspondingly and spontaneously due to the significant difference in bond energies between hydrogen bond and coordinate bond: all or part of connections between MA and TMA originally on the basis of the hydrogen bonding interaction could be replaced by the stronger covalent interaction between the uranyl ions and the N-, O-containing ligands in the heterocyclic framework self-assembled from MA and TMA. As a result, a new and more stable MA-UO_2^{2+}-TMA type chelate-based MA-TMA-U is formed with coordination number most likely to be 4. In the framework of MA-TMA-U, uranyl ions act as bridging or linking units between MA and TMA. So a possible coordination mechanism between MA-TMA and uranyl ion in the extraction process was proposed and shown in Scheme 2.

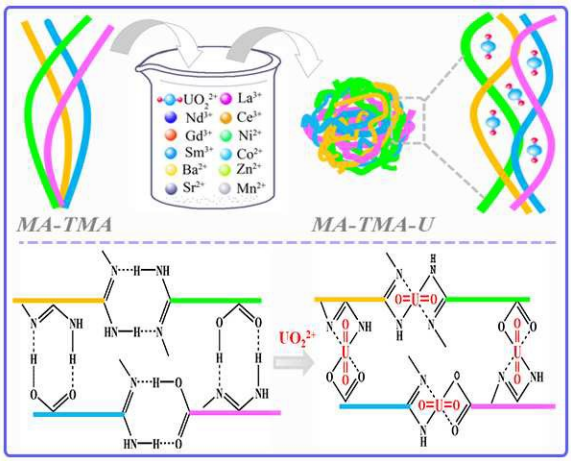

Scheme 2 Possible mechanism of uranium extraction by MA-TMA

Briefly speaking, we believe that the above "in situ induced-fit ion recognition" mechanism leads to high selectivity in the uranyl extraction based on both the unique feature of uranyl coordination chemistry and the flexible hydrogen-bonded SOF-based adsorbent that could responsively change its chemical bonding between the building blocks when encountering uranyl ion. However, it's possible that a small amount of terminal groups, such as amino and /or hydroxyl group located in the edge of the MA-TMA framework, could also have coordination interaction with uranyl ions, but the ion selectivity and the complex stability in these process are not better than that in the induced-fit process, and moreover, the two axial oxygen atoms of uranyl ion might form hydrogen bonds with the amino and/or hydroxyl groups located on adjacent layers of the MA-TMA framework.

4. Conclusion

In summary, an adaptive SOF-based SPE adsorbent (MA-TMA) has been successfully prepared on the concept of "induced-fit ion recognition". MA-TMA shows excellent selectivity, specific recognition ability and large adsorption capacity towards uranium, which preferably solved the problems of unsatisfactory selectivity and/or lower adsorption capacity that exist in the previously-reported uranium-specific SPE sorbents. Herein, a right combination of the three crucial factors, involving the bifunctionality of the building blocks (MA and TMA), the reversible, adaptive and flexible nature of the SOF-based adsorbent built through inter-molecular hydrogen bonding between the building blocks, and the unusual coordination geometry of UO_2^{2+}, provides the structural and functional basis of MA-TMA for the high-efficiency separation of uranium and the self-crimping and aggregation in the course of extraction of UO_2^{2+} onto MA-TMA.

The results of our batch experiments indicate that the uranium adsorption on MA-TMA is a spontaneous, exothermic, fast and a pseudo-second order process. Furthermore, the as-synthesized SOF-based SPE sorbent has its significant practical advantages, such as readily accessible cheap starting materials, convenient one-step process for preparation with mild conditions and scalable potential. The findings demonstrate that MA-TMA is among the most attractive adsorbent for uranium, and has great potential applications in the highly efficient separation and recovery of uranium from various uranium-containing systems (mining wastewater, nuclear industrial effluents, salt lake and seawater etc.). Meanwhile, the design strategy used in this work may also provide a new and alternative approach for the rational design and preparation of other intelligent SOFs materials with promising applications in selective recognition of other desired metal ions.

Acknowledgements

The financial support from the National Natural Science Foundation of China (Grants 21171122, 21271132, 11475120, J1210004 and J1103315) are gratefully acknowledged.

References

Journal of Materials Chemistry A Accepted Manuscript

1. M. J. Manos and M. G. Kanatzidis, *J. Am. Chem. Soc.*, 2012, **134**, 16441.
2. H. Wang, L. J. Ma, K. C. Cao, J. X. Geng, J. Liu, Q. Song, X. D. Yang and S. J. Li, *J. Hazard. Mater*., 2012, **229**, 321.
3. X. P. Liao, Z. B. Lu, X. Du, X. Liu and B. Shi, *Environ. Sci. Technol*., 2004, **38**, 324.
4. E. R. Sylwester, E. A. Hudson and P. G. Allen, *Geochim. Cosmochim. Acta*, 2000, **64**, 2431.
5. R. P. Han, W. H. Zou, Y. Wang and L. Zhu, *J. Environ. Radioact*., 2007, **93**, 127.
6. S. Aytas, M. Yurtlu and R. Donat, *J. Hazard. Mater*., 2009, **172**, 667.
7. L. M. Camacho, S. G. Deng and R. R. Parra, *J. Hazard. Mater*., 2010, **175**, 393.
8. T. D. Waite, J. A. Davis, T. E. Payne, G. A. Waychunas and N. Xu, *Geochim. Cosmochim. Acta*, 1994, **58**, 5465.
9. S. E. Bailey, T. J. Olin, R. M. Bricka and D. D. Adrian, *Water Res*., 1999, **33**, 2469.
10. S. Y. Bae, G. L. Southard and G. M. Murray, *Anal. Chim. Acta*, 1999, **397**, 173.
11. I. Zhuravlev, O. Zakutevsky, T. Psareva, V. Kanibolotsky, V. Strelko, M. Taffet and G. Gallios, *J. Radioanal. Nucl. Chem*., 2002, **254**, 85.
12. P. Misaelides, G. Gallios, S. Sarri, D. Zamboulis, E. Pavlidou, N. Kantiranis, I. Anousis, I. Zhuravlev and V. Strelko, *Sep. Sci. Technol*., 2006, **41**, 97.
13. C. R. Preetha, J. M. Gladis, T. P. Rao and G. Venkateswaran, *Environ. Sci. Technol*. , 2006, **40**, 3070.
14. S. J. Ahmadi, N. K. Omid and S. A. Simindokht, *J. Hazard. Mater*., 2010, **175**, 193.
15. N. Seko, A. Katakai, M. Tamada, T. Sugo and F. Yoshii, *Sep. Sci. Technol*., 2004, **39**, 3753.
16. A. Zhang, T. Asakura and G. Uchiyama, *React. Funct. Polym*., 2003, **57**, 67.
17. N. Kabay and H. Egawa, *Sep. Sci. Technol*., 1994, **29**, 135.
18. X. D. Yang, J. Li, J. Liu, Y. Tian, B. Li, K. C. Cao, S. B. Liu, M. Hou, S. J. Li and L. J. Ma, *J. Mater. Chem. A*, 2014, **2**, 1550.
19. J. Górka, R. T. Mayes, L. Baggetto, G. M. Veith and S. Dai, *J. Mater. Chem. A*, 2013, **1**, 3016.
20. S. Y. Xie, X. Y. Liu, B. W. Zhang, H. J. Ma, C. J. Ling, M. Yu, L. F. Li and J. Y. Li, *J. Mater. Chem. A*, 2015, **3**, 2552.
21. P. J. Lebed, J.-D. Savoie, J. Florek, F. o. Bilodeau, D. Larivière and F. Kleitz, *Chem. Mater*., 2012, **24**, 4166.
22. L. Y. Yuan, Y. L. Liu, W. Q. Shi, Z. J. Li, J. H. Lan, Y. X. Feng, Y. L. Zhao, Y. L. Yuan and Z. F. Chai, *J. Mater. Chem*., 2012, **22**, 17019.
23. J. Li, X. D. Yang, C. Y. Bai, Y. Tian, B. Li, S. Zhang, X. Y. Yang, S. D. Ding, C. Q. Xia and X. Y. Tan, *J. Colloid Interface Sci*., 2015, **437**, 211.
24. Z. Q. Bai, L. Y. Yuan, L. Zhu, Z. R. Liu, S. Q. Chu, L. R. Zheng, J. Zhang, Z. F. Chai and W. Q. Shi, *J. Mater. Chem. A*, 2015, **3**, 525.
25. F. Luo, L. L. Dang, J. Q. Li, S. juan Liu, M. B. Luo and L. L. Wang, *J. Mater. Chem. A*, 2015, **3**, 13724.
26. M. Carboni, C. W. Abney, S. B. Liu and W. B. Lin, *Chem. Sci*., 2013, **4**, 2396.
27. L. Zhou, M. Bosscher, C. S. Zhang, S. Özçubukçu, L. Zhang, W. Zhang, C. J. Li, J. Z. Liu, M. P. Jensen and L. H. Lai, *Nat. Chem*., 2014, **6**,236.
28. L. Ling and W. x. Zhang, *J. Am. Chem. Soc*., 2015, **137**, 2788.
29. S. L. Ma, L. Huang, L. J. Ma, Y. Shim, S. M. Islam, P. L. Wang, L. D. Zhao, S. C. Wang, G. B. Sun and X. J. Yang, *J. Am. Chem. Soc*., 2015, **137**, 3670.
30. R. Ruhela, N. Iyer, M. Yadav, A. K. Singh, R. C. Hubli and J. K. Chakravartty, *Green Chem*., 2015, **17**, 827.
31. T. A. Davis, B. Volesky and A. Mucci, *Water Res*., 2003, **37**, 4311.
32. B. Li, L. Ma, Y. Tian, X. D. Yang, J. Li, C. Y. Bai, X. Y. Yang, S. Zhang, S. J. Li and Y. D. Jin, *J. Hazard. Mater*., 2014, **271**, 41.
33. G. N. Greaves, N. T. Barrett, G. M. Antonini, F. R. Thornley, B. T. M. Willis and A. Steel, *J. Am. Chem. Soc*., 1989, **111**, 4313.
34. J. Lü, C. Perez-Krap, M. Suyetin, N. H. Alsmail, Y. Yan, S. Yang, W. Lewis, E. Bichoutskaia, C. C. Tang and A. J. Blake, *J. Am. Chem. Soc*., 2014, **136**, 12828.
35. J. M. Lehn, *Angew. Chem. Int. Ed*., 1990, **29**, 1304.
36. C. Michaelá Drain, *Chem. Commun*., 1996, 337.
37. S. Hanessian, M. Simard and S. Roelens, *J. Mater. Chem. A*, 1995, **117**, 7630.
38. F. W. Zeng and S. C. Zimmerman, *Chem. Rev*., 1997, **97**, 1681.
39. W. B. Yang, A. Greenaway, X. Lin, R. Matsuda, A. J. Blake, C. Wilson, W. Lewis, P. Hubberstey, S. Kitagawa and N. R. Champness, *J. Am. Chem. Soc*., 2010, **132**, 14457.
40. Y. B. He, S. C. Xiang and B. L. Chen, *J. Am. Chem. Soc*., 2011, **133**, 14570.
41. P. Li, Y. B. He, J. Guang, L. H. Weng, J. C. G. Zhao, S. C. Xiang and B. L. Chen, *J. Am. Chem. Soc*., 2014, **136**, 547.
42. D. L. Wang, Y. Su, C. Y. Jin, B. S. Zhu, Y. Pang, L. J. Zhu, J. Y. Liu, C. L. Tu, D. Y. Yan and X. Y. Zhu, *Biomacromolecules*, 2011, **12**, 1370.
43. Q. P. Duan, Y. Cao, Y. Li, X. Y. Hu, T. X. Xiao, C. Lin, Y. Pan and L. Y. Wang, *J. Am. Chem. Soc*., 2013, **135**, 10542.
44. X. F. Ji, Y. Yao, J. Y. Li, X. Z. Yan and F. H. Huang, *J. Am. Chem. Soc*., 2012, **135**, 74.
45. W. H. James III, C. W. Müller, E. G. Buchanan, M. G. D. Nix, L. Guo, L. Roskop, M. S. Gordon, L. V. Slipchenko, S. H. Gellman and T. S. Zwier, *J. Am. Chem. Soc*., 2009, **131**, 14243.
46. H. S. Lee, Y. K. Wang and S. L. Hsu, *Macromolecules*, 1987, **20**, 2089.
47. Q. Huo, L. Dziri, B. Desbat, K. Russell and R. M. Leblanc, *J. Phys. Chem. B*, 1999, **103**, 2929.
48. Y. S. Jun, E. Z. Lee, X. C. Wang, W. H. Hong, G. D. Stucky and A. Thomas, *Adv. Funct. Mater*., 2013, **23**, 3661.
49. H. J. Jeon, S. C. Yi and S. G. Oh, *Biomater*., 2003, **24**, 4921.
50. F. H. Beijer, H. Kooijman, A. L. Spek, R. P. Sijbesma and E. W. Meijer, *Angew. Chem. Int. Ed*., 1998, **37**, 75.
51. D. E. Giammar and J. G. Hering, *Environ. Sci. Technol.* , 2001, **35**, 3332.
52. S. Amayri, T. Arnold, T. Reich, H. Foerstendorf, G. Geipel, G. Bernhard and A. Massanek, *Environ. Sci. Technol.* , 2004, **38**, 6032.
53. T. Classen, M. Lingenfelder, Y. Wang, R. Chopra, C. Virojanadara, U. Starke, G. Costantini, G. Fratesi, S. Fabris and S. Gironcoli, *J. Phys. Chem. A*, 2007, **111**, 12589.
54. C. C. Ji, J. Li, Y. Z. Li and H. G. Zheng, Inorg. *Chem. Commun*., 2010, **13**, 1340.
55. W. Chen, H. M. Yuan, J. Y. Wang, Z. Y. Liu, J. J. Xu, M. Yang and J. S. Chen, *J. Am. Chem. Soc*., 2003, **125**, 9266.
56. W. T. Yang, Z. Q. Bai, W. Q. Shi, L. Y. Yuan, T. Tian, Z. F. Chai, H. Wang and Z. M. Sun, *Chem. Commun*., 2013, **49**, 10415.
57. Q. Song, L. J. Ma, J. Liu, C. Y. Bai, J. X. Geng, H. Wang, B. Li, L. Y. Wang and S. J. Li, *J. Colloid Interface Sci*., 2012, **386**, 291.
58. J. Qu, W. Li, C. Y. Cao, X. J. Yin, L. Zhao, J. Bai, Z. Qin and W. G. Song, *J. Mater. Chem*., 2012, **22**, 17222.

Journal of Materials Chemistry A Accepted Manuscript

This journal is © The Royal Society of Chemistry 20xx

四川大學
SICHUAN UNIVERSITY
DEPARTMENT OF CHEMISTRY

Graphical and Abstract

An adaptive supramolecular organic framework for highly efficient separation of uranium via in situ induced fit mechanism

Bo Li, Chiyao Bai, Shuang Zhang, Xiaosheng Zhao, Yang Li, Lei Wang, Kuan Ding, Xi Shu, Shoujian Li* and Lijian Ma*

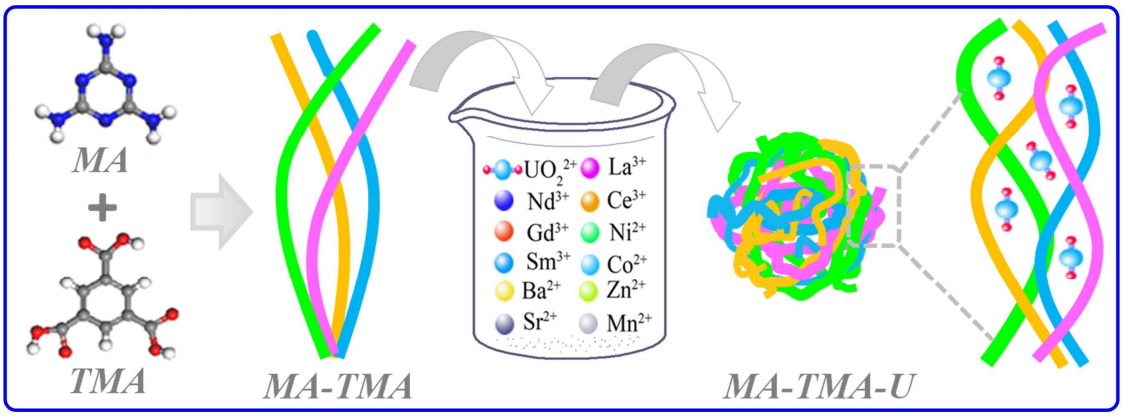

The as-synthesized adaptive supramolecular organic framework (MA-TMA) filled with abundant hydrogen-bonded N-/N and N-/O-heterocyclic motifs exhibits remarkable ability for highly efficient separation of uranium via in-suit “induced-fit” ion recognition mechanism.

Journal of Materials Chemistry A Accepted Manuscript